25th ABCM International Congress of Mechanical Engineering
October 20-25, 2019, Uberlândia, MG, Brazil

COB-2019-2371
DEPOSITION OF ALUMINA ON ANSI 304 STAINLESS STELL BY PLASMA POWDER SPRAY

Roberson José da Silva
Felipe de Souza Miranda
Homero Santiago Maciel
Gilberto Petraconi Filho
Instituto Tecnológico de Aeronáutica, São José dos Campos, SP, Brasil
roberson123@gmail.com , mirannda.fs@gmail.com, odairtur@gmail.com, petrafilho@gmail.com

Abstract. *Aerospace and aeronautics applications require some special features, such as high temperature work and ablation resistance. Ceramic materials have been increasingly used in these applications because they have advantages over metals in these requirements. On the other hand, metals still constitute several important structural features that cannot simply be replaced. Thus, the ceramic coating of metal parts has been an interesting alternative to add thermal and ablative resistance to the metal part. This work presents studies on thermal spraying technique to deposit alumina powder on metallic substrate by using a thermal plasma torch of long arc. This system applied a plasma heat flow at 5,100 °C to melt an alumina powder and to coat a metallic substrate of ANSI 304 stainless steel. The e parameters of spraying process was adjusted in order to obtain the complete fusion of the powder grains and to obtained a thickness of coating about 100 μm. The coated sample was analyzed by profilometry, X-ray diffraction and SEM / EDS.*

Keywords: *aerospace, aeronautics, ceramic coating, plasma spray, thermal spray*

1. INTRODUCTION

Plasma Spray emerged after Second World War as a surface finishing technology. Nowadays it is widely used for the deposition of thick coatings (from hundreds of micrometers up to a few millimeters) in a substrate for protection in an aggressive environment or to improve its function. The large numbers of industrial processes operating in the highly aggressive environments are characterized due to high temperature, pressure and stress on the elements that integrate the system. It is commonly used in many industrial sectors, including aeronautics, energy, automotive, mining, biomedical and electronics (Tucker Jr., 2013).

In the aeronautics industry, for example, fuel is injected into the turbines and combustion causes an increase in pressure and temperature. In the exhaust nozzle temperatures can reach 1,650 °C, and during their cooling they remain in contact with the atmosphere becoming susceptible to oxidation (Sethi and Wright, 1991). Particulate materials and the presence of oxidizing and corrosive atmospheres contribute to system failure. Turbines, oil refineries and nuclear power plants have high temperature and oxidation as the main failure mechanisms (Miranda et al., 2018). To protect these systems, several studies aimed at surface layer deposition are being carried out, with the primary objective of preventing the base material from being submitted directly to the aggressive environment and losing its specific and desired properties (Lee, 2000).

In the plasma spray technique, a carrier gas conducts the particles of the material by injecting them at high velocity through the plasma, where they are molten or partially molten, in the form of droplets which settle and solidify on the surface to be coated (Fauchais, 2004; Xie et al., 2004). The process parameters as well as the characteristics of the precursor used for the coating influence the properties of the deposited materials. For example, high plasma jet temperatures and high cooling rates of the material during the coating process can also promote the formation of amorphous phases (Sampath and Jiang, 2001; Cao et al., 2004). Characteristics of the coatings as porosity, atomic structure, roughness, cohesion and adhesion are fundamentally related to the effect of the interaction of the precursor with the plasma jet (Guo et al., 2005; Xie et al., 2006).

The synthesis of coatings by the plasma spray deposition technique occurs by stacking the lamellae resulting from impact, flattening and solidification by the collision of molten particles (Xie et al., 2004). What distinguishes the plasma spray process from other technologies is their applicability to a wide variety of materials, including metallic and ceramic materials. The main driving force for the manufacture of thick plasma spray coatings is their high deposition

rate. Some kilograms per hour of raw material can be processed with torches with a power level of a few tens of kilowatts at a relatively low operating cost. Plasma spray is probably the most versatile of all thermal spraying processes, because there are few limitations of materials that can be sprayed, and few limitations on the material, size and shape of the substrate (Fauchais, 2004).

The protective coatings against oxidation and corrosion are typically aluminum based materials, aiming at the formation of aluminum oxide in its final composition (Miranda et al., 2018). In this context this work presents the studies about the effect of the plasma spray parameters on the chemical and physical properties of alumina coatings on ANSI 304 stainless steel.

2. MATERIALS AND METHOLDS

2.1. Materials

The ceramic powder used in the spraying was alumina with granulometry of 70–210 μm. This alumina was previously heated in an oven at 60 °C for 4 hours and then sieved to define this range of granulometry. The substrates used were ANSI 304 stainless steel, disk-shaped, 45 mm in diameter and 4 mm thick. Figure 1 shows the substrate (a) and the alumina powder (b) that were used.

Figure 1. ANSI 304 stainless steel substrate (a) and 70–210 μm alumina powder (b)

2.2. Thermal powder spray system

The plasma torch was adjusted to an inlet gas flow rate of 90 L/min (air) and a current of 105 A (30 kW), generating a supersonic air jet with specific enthalpy of 11 MJ/kg at the torch nozzle. At this enthalpy the gas in the plasma jet at the nozzle of the torch reaches temperature about 5,100 °C (P. Fauchais; M. I. Boulos and E. Pfender, 1994). The alumina melting point is 2,072 ° C (Patnaik, 2003) and this plasma temperature is sufficient to promote melted of the powder in a short residence time in the plasma jet. The 6 mm diameter plasma jet output provides a supersonic velocity of about 500 m/s for molten powder particles.

Powder injection was performed by a Tekna model PFV 101 vibratory powder feeder. The powder feeder was set to 3–5 g/min powder flow rate at 114.8 Hz and 11% vibration intensity. The carrier gas flow rate (air) was adjusted to 5 L/min.

2.3. Spraying tests

The substrate was positioned at 65 mm from the plasma torch nozzle after the operational conditions stabilization as shown in Figure 2. Three substrate samples were covered and in each one them was performed 8 depositions layers, interspersed with a time of 3 min cooling. The spray time per layer in each sample A15, A16 and A17 was 4, 5 and 6 s, respectively.

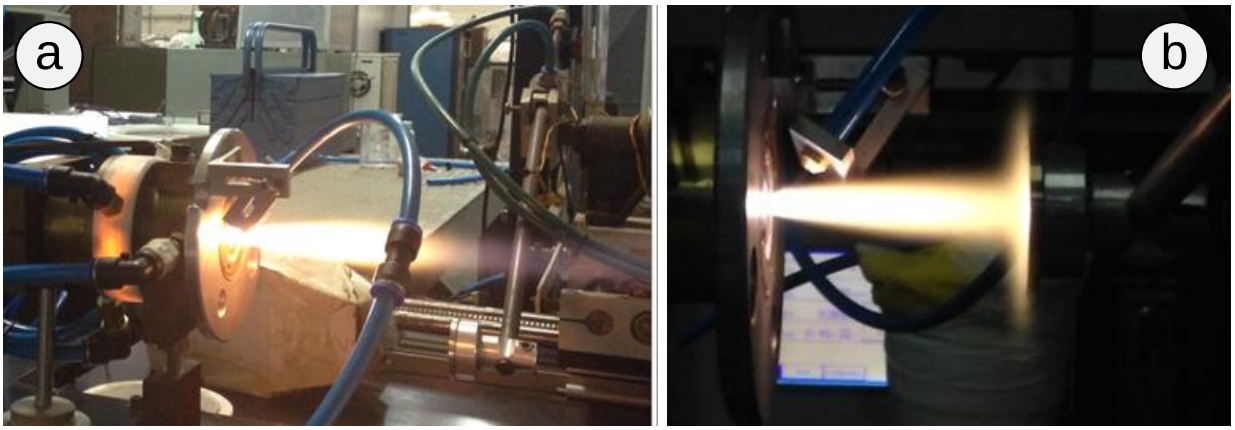

Figure 2. (a) Image of the plasma spray system and (b) process region

2.4. Analises of the coatings

After coating, the coated samples were analyzed with a mechanical profile profilometer model P 7 Stylus Profiler from KLA Tencor where the coating profile, the maximum thickness, the presence of cracks and discontinuities in the film were verified.

Microstructural analysis was performed using a Tescan Vega 3 XMU scanning electron microscope (SEM) equipped with Philips PW1830 / 1840 for energy dispersive X-ray spectroscopy (EDS). Experimental diffractograms were compared with a library of theoretical diffractograms and selected according to suitability for the material analyzed.

3. RESULTS

Figure 3 shows the result obtained with the coating of samples A15, A16 and A17 corresponding to the spray exposure times per layer of 4, 5 and 6 s, respectively.

Figure 3. A15, A16 and A17 samples after thermal spray coating

It is possible to observe that sample A15 presented the most homogeneous coating, with no apparent defects. In A16 sample was noticed a slight overhang on surface coating. Sample A17 showed a slight discontinuous lifting of the coating as a possible crack.

3.1. Profilometry

The profilometry results are shown in the Figure 4. It were obtained thicknesses coat peak of 60–110 μm increasing with the deposition time per layer. It can be seen that using a longer time of deposition per layer gives a thicker coating, but the excess heat in the substrate results to cracks coating caused mainly by the difference in the coefficients of thermal expansion of the metallic substrate and the ceramic coating (Cao et al., 2004).

In sample A17 the highest coating thickness was obtained, but the crack that could already be seen in figure 3 was evidenced by a large degree of discontinuity on the horizontal left side of the scan profile in Figure 4. As it was shown in figure 3, A16 sample showed only a slight overhang, i.e., a complete crack did not occur to relieve the stresses resulting from the thermal contraction of the metal during cooling as in A17. Thus, microcracks occurred in a larger region for stress relief, covering both profiles. In sample A15 there was less heating of the substrate and due to this there was no visual defect. Even so, the discontinuities are present in the horizontal scan profile showing possible microcracks as in A16, but in smaller number and intensity.

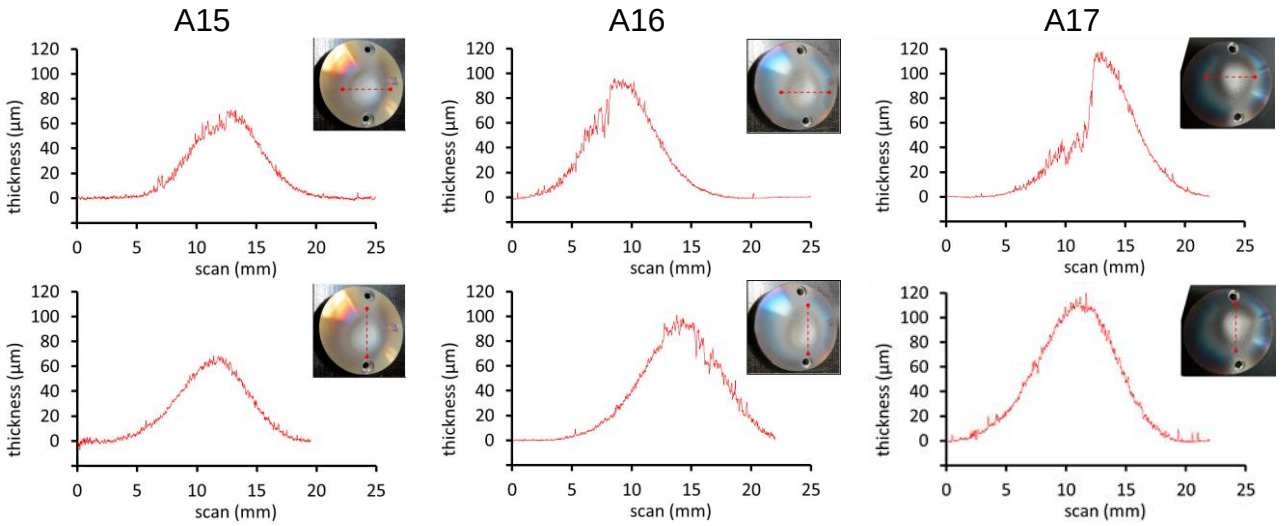

Figure 4. Profile of samples A15, A16 and A17 for the deposition times per layer of 4, 5 and 6 s

3.2. X-ray difratometry

Figure 5 shows the X-ray diffraction analysis of the alumina powder (a), of the A15 coated sample (b) and the ANSI 304 substrate without coating (c). It was found that the spectra in sample A15 coincide with the spectral junction of the alumina powder and the (attenuated) substrate. The alumina-α peaks remain thin and defined in the coated sample, showing that a crystalline alumina structure (α) is present in the coating.

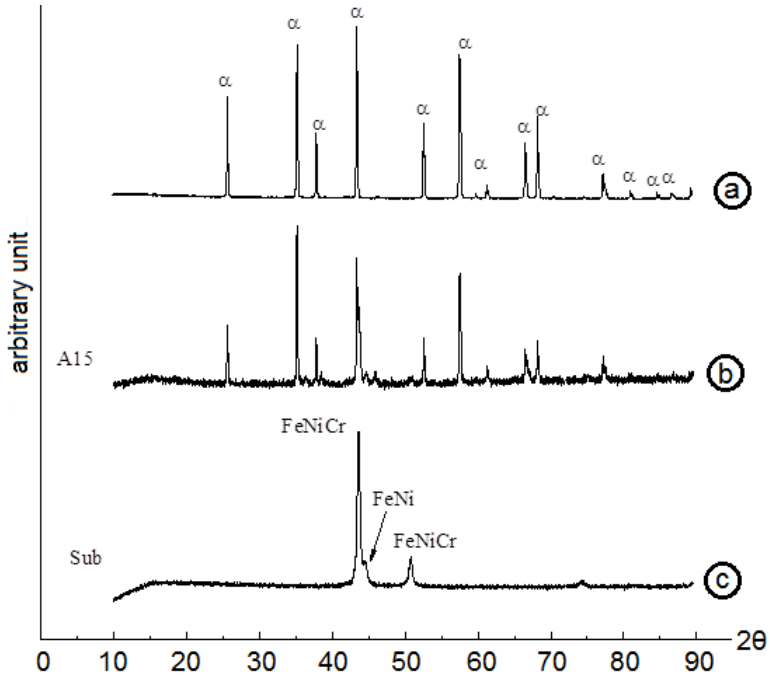

Figure 5. X-ray diffraction: diffractograms of alumina powder (a), A15 sample coating (b) and ANSI 304 substrate (c)

3.3. Microscopy – SEM and EDS

Figure 6 shows the microstructure of a grain of this powder obtained by SEM. It can be seen that this grain about 100 µm is formed by many microplatelets with diameter varying in the range of 1–5 µm (b). An important observed characteristic is its polygonal shape with corners and straight edges that will be change after thermal spraying.

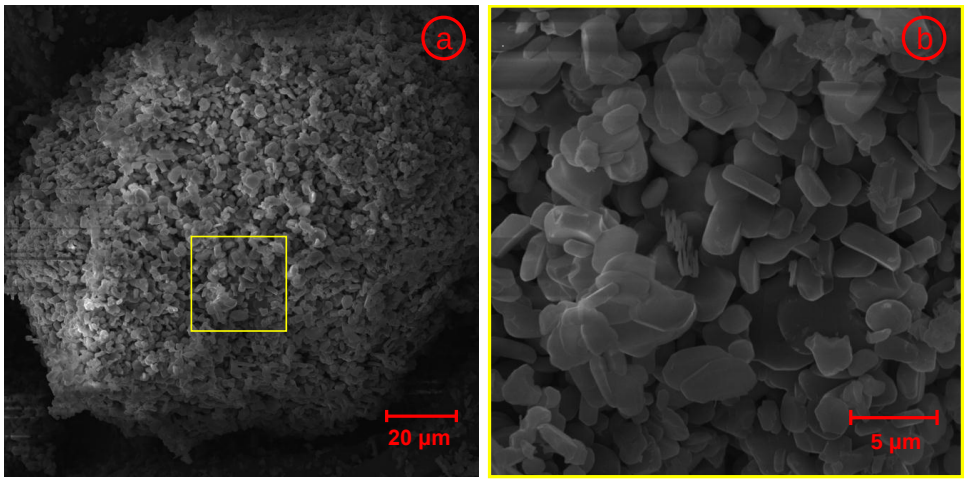

Figure 6. Alumina powder grain of 75–210 µm

Sample A15, after non-destructive testing, was prepared for microstructural analysis. The sample thickness was reduced to 3 mm and two circular segments were removed leaving only the disc strip where there was coating. Using a diamond disc, this strip was cut into two parts by dividing the coating profile into two halves: A15-1 and A15-2. A15-1 was used for surface analysis and A15-2 for layer cross section analysis. Figure 7 shows the microstructural analysis performed on sample A15-1.

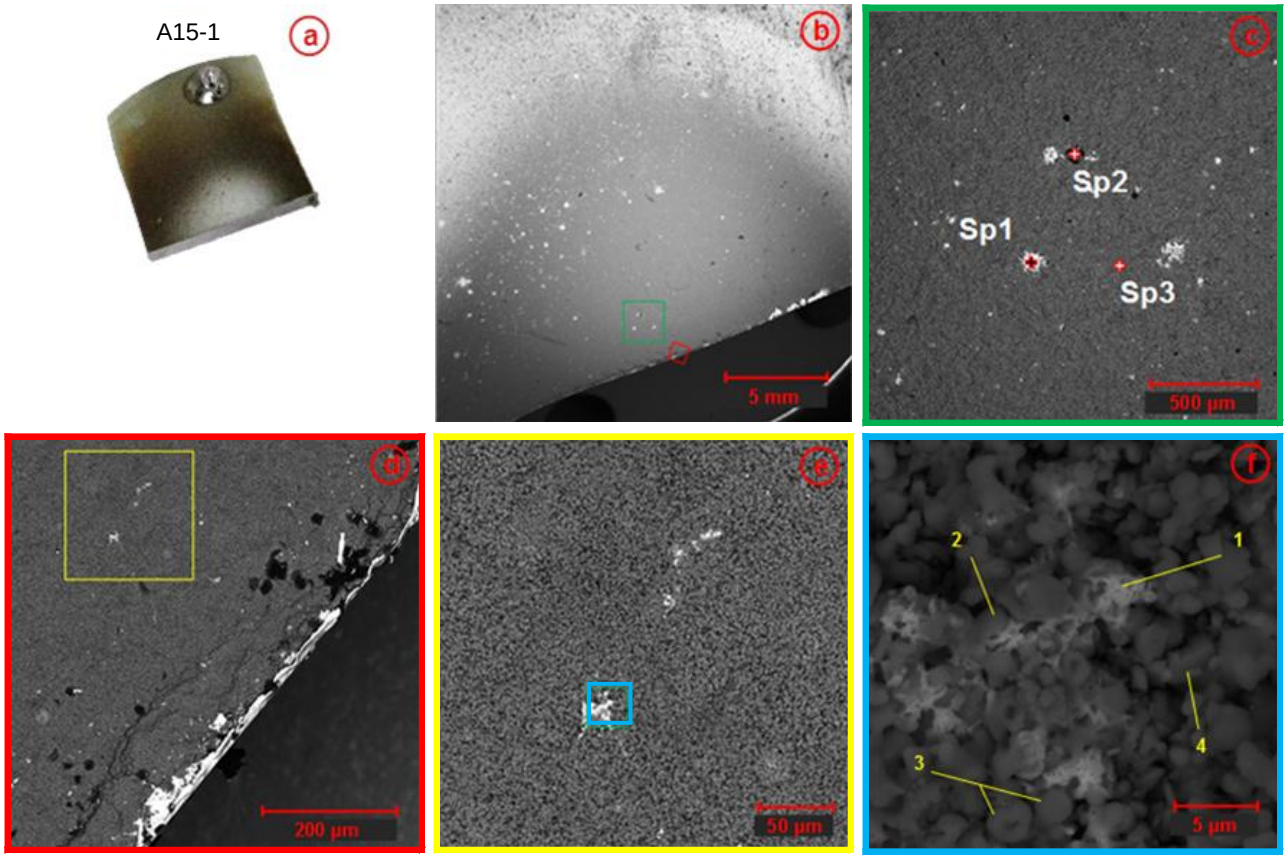

Figure 7. SEM analysis of the coating surface in A15-1 sample

Two regions are identified with colored rectangles in micrograph (b): one near the peak deposition region (c) and another at the cutting edge of the sample (d). In ‘d’ it is possible to see the cracks caused at the edge due to cutting with the diamond blade. At ‘e’ magnification it is possible to identify a light smudge on a grainy surface. In detail ‘f’, the light smudge can be seen as a molten material (1) and mixed with the coating alumina grains. The alumina grains have been melted and adhered to the coating (2) or at least they were fused partially showing now a more rounded aspect (3).

But a small portion still remains with polygonal aspect and evident edges showing that they not were melted (4). In micrograph 'c', 3 points with different formations were identified and analyzed by EDS: Sp1 in the granular region of the coating, Sp2 in a dark smudge and Sp3 in the light smudge. Figure 8 shows the element spectrums that were identified by EDS analysis.

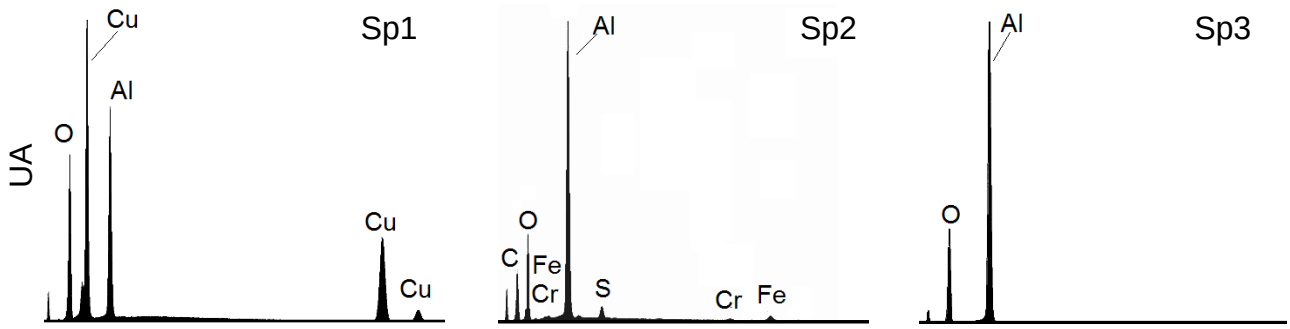

Figure 8. EDS analysis of the coating surface in A15-1 sample

In Sp1 there is the presence of alumina elements (Al and O) and also copper from the erosion processes of the torch electrodes by plasma. In Sp2 it was possible to identify some elements of substrate alloy and the alumina. This shows the dark spot is a failure region on coating where the substrate is more exposed. In Sp3, as expected, only alumina elements are detected.

Figure 9 shows the microstructural analysis performed on A15-2.

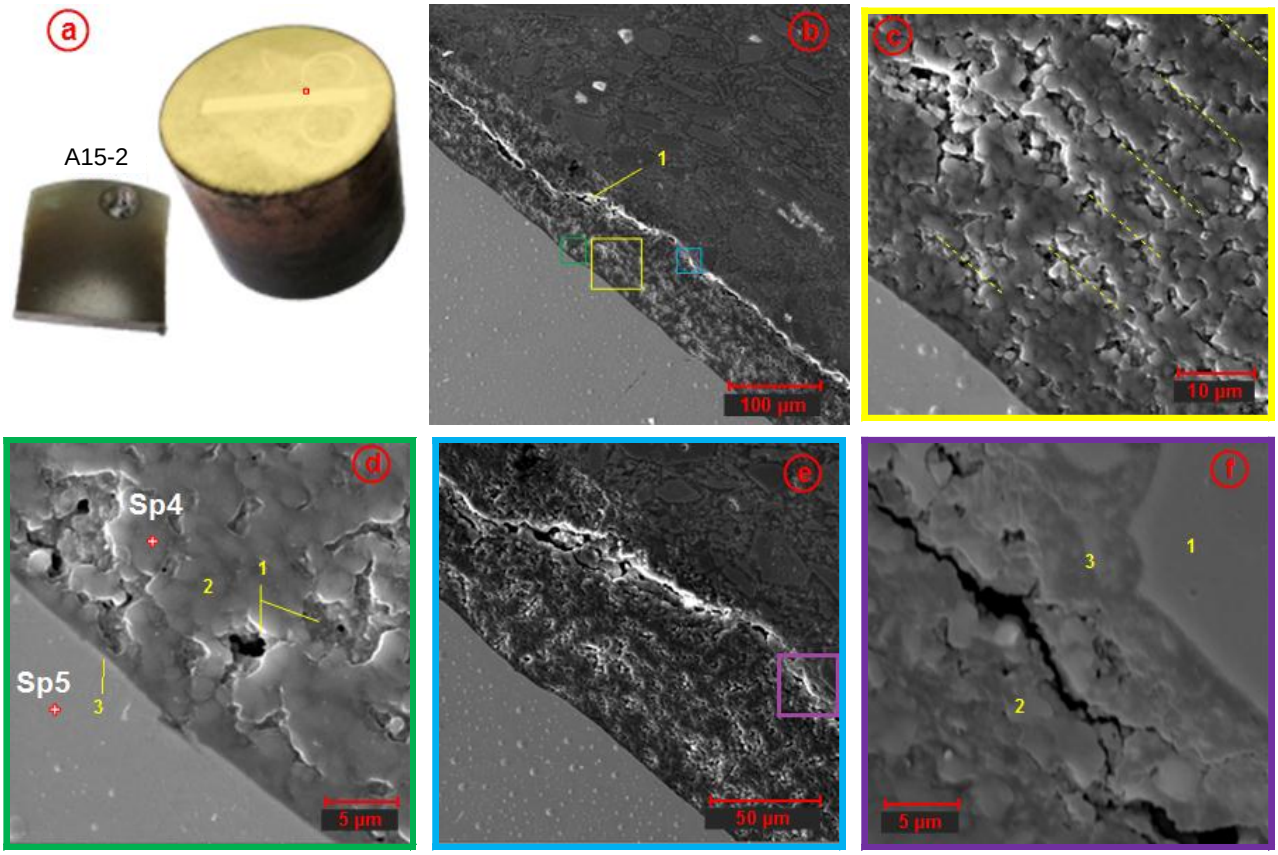

Figure 9. SEM analysis of the coating layers in A15-2 sample

This sample was embedded in Bakelite and polished in the cutting region for visualization of the microstructure of ceramic coating layers and the interface region with the metallic substrate. A gold thin coating was applied to the polished surface (a) to make it conductive and thus obtain a better SEM sharpness. In the first magnification (b) three distinct regions can be identified: the substrate in the lighter region, the alumina coating in the central diagonal strip and the Bakelite above. The thickness of the coating corresponds to the results of the profilometry of approximately 60 µm.

A crack can be observed in the inner layers of the coating. This crack propagates between the layers and reaches the coating surface (1). The rectangle marks correspond to detailed micrographs in these regions. In “c”, the segmented lines indicate an alignment pattern of the porosities that correspond to interface between alumina layers that were deposited. The micrograph 'd' shows the coating microstructure with the voids (1) and fills (2) areas. The coating fill area is formed by a mixture melted alumina and non-melded alumina grains (2). At interface between the coating and the substrate it is verified low porosity and no detachment (3). In micrographs 'e' and 'f' details of the crack region are shown. In 'f' it can be seen that Bakelite (1) penetrated the porous surface of the alumina coating (2) creating a mixed interface region (3). After cooling of the embedding, Bakelite retraction may have contributed to the crack propagation already evidenced in profilometry analyzes, causing shedding of the coating layers. In this case, it would be more appropriate to use a cold embedding in order not to influence in layers detachment of the coating.

An important fact to note is that cracking occurred between layers and not at the interface of the coating with the substrate. This indicates that the adhesion of the first alumina layer to the substrate is better than between the alumina layers of the coating.

Figure 10 shows the EDS analysis performed on alumina coating (Sp4) and substrate (SP5) as indicated in figure 9. In Sp4, as expected, the alumina elements (Al and O) were evidenced. In Sp5, the main elements that make up the ANSI 304 alloy (Cr, Ni and Fe) were found. In both spectrum scans, gold peaks used in the surface preparation of sample A15-2 were found.

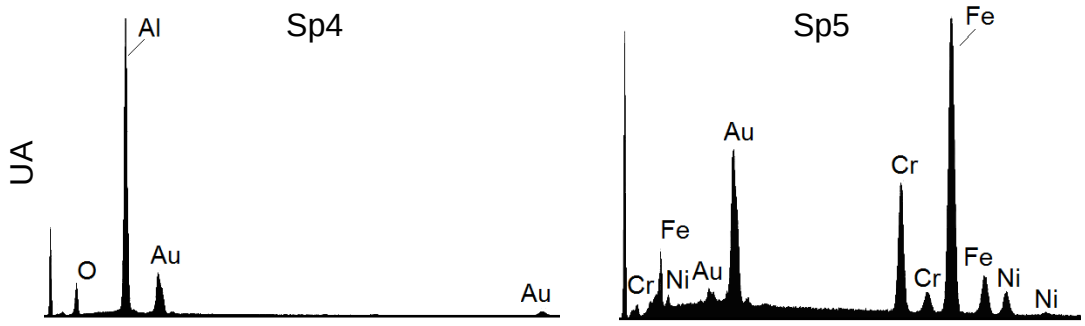

Figure 10. EDS analysis of the coating layers in A15-2 sample

4. CONCLUSIONS

Through the performed studies it was verified that the conditions used in the spray were sufficient to promote the fusion of the platelets from alumina powder, generating a film adhered to the ANSI 304 stainless steel metal substrate, although still very porous. It has also been found that the difference in the coefficient of thermal expansion between the substrate and the coating is a critical factor to be considered, as it is directly linked to the origin of the cracking and detachment in the coating. This characteristic proved to be a bottleneck in obtaining thicker films. The achievement of uniform, thick, dense and adhered ceramic coatings using plasma thermal spray requires the control of various parameters and techniques that constitute the thermal spraying process in order to minimize cracking and porosity.

5. ACKNOWLEDGEMENTS

The authors would like to thank the Brazilian Space Agency (AEB) and the National Council for Scientific and Technological Development (CNPq) for funding the research.

6. REFERENCES

Cao X.Q., Vassen R., Stoever D., 2004. "Ceramic materials for thermal barrier coatings". *J Eur Ceram Soc*, Vol. 24, pp. 1–10

Fauchais P., 2004. "Understanding plasma spraying". *J Phys D Appl Phys*, Vol. 37, pp. R86–R108

Guo F.A., Trannoy N., Gerday D., 2005. "An application of scanning thermal microscopy: Analysis of the thermal properties of plasma-sprayed yttria-stabilized zirconia thermal barrier coating". *J Eur Ceram Soc*, Vol. 25, pp. 1159–1166

Lee K.N., 2000. "Current status of environmental barrier coatings for Si-Based ceramics". *Surf Coatings Technol*, Vol. 133–134, pp. 1–7

Miranda F., Caliari F., Essiptchouk A., Pertraconi G., 2018. "Atmospheric Plasma Spray Processes: From Micro to Nanostructures". In: Atmospheric Pressure Plasma [Working Title]. IntechOpen

P. Fauchais; M. I. Boulos and E. Pfender, 1994. Thermal Plasmas - Fundamentals and Applications, volume 1. New York

Patnaik P., 2003. Handbook of Inorganic Chemicals

Sampath S., Jiang X., 2001. "Splat formation and microstructure development during plasma spraying: deposition temperature effects". *Mater Sci Eng A*, Vol. 304–306, pp. 144–150

Sethi V.J., Wright I.G., 1991. "Corrosion-Erosion-Wear of Materials at High Temperatures". In: Levy A V. (ed) Proceedings of the Conference on Corrosion–Erosion. Houstan, TX, p 18

Tucker Jr. R.C., 2013. ASM Handbook, Volume 05A - Thermal Spray Technology

Xie L., Chen D., Jordan E.H., Ozturk A., Wu F., Ma X., Cetegen B.M., Gell M., 2006. "Formation of vertical cracks in solution-precursor plasma-sprayed thermal barrier coatings". *Surf Coatings Technol*, Vol. 201, pp. 1058–1064

Xie L., Ma X., Ozturk A., Jordan E.H., Padture N.P., Cetegen B.M., Xiao D.T., Gell M., 2004. "Processing parameter effects on solution precursor plasma spray process spray patterns". *Surf Coatings Technol*, Vol. 183, pp. 51–61

7. RESPONSIBILITY NOTICE

The authors are the only responsible for the printed material included in this paper.